Article

Principal Active Species of Horseradish Peroxidase, Compound I: A Hybrid Quantum Mechanical/Molecular Mechanical Study

Etienne Derat, Shimrit Cohen, Sason Shaik, Ahmet Altun, and Walter Thiel

J. Am. Chem. Soc., **2005**, 127 (39), 13611-13621• DOI: 10.1021/ja0534046 • Publication Date (Web): 13 September 2005

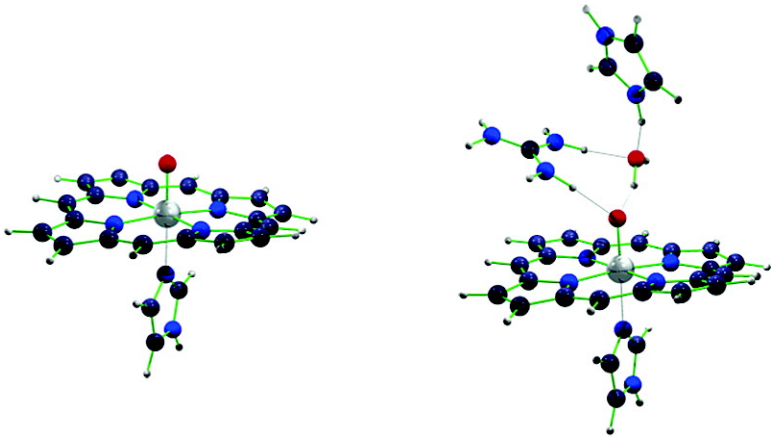

J|A|C|S
ARTICLES
Published on Web 09/13/2005

Principal Active Species of Horseradish Peroxidase, Compound I: A Hybrid Quantum Mechanical/Molecular Mechanical Study

Etienne Derat,[†] Shimrit Cohen,[†] Sason Shaik,*[,†] Ahmet Altun,[‡] and Walter Thiel[‡]

Contribution from the Institute of Chemistry and the Lise-Meitner-Minerva Center for Computational Quantum Chemistry, The Hebrew University of Jerusalem, 91904 Jerusalem, Israel, and Max-Planck-Institut für Kohlenforschung, Kaiser-Wilhelm-Platz 1, D-45470 Mülheim an der Ruhr, Germany

Received May 25, 2005; E-mail: sason@yfaat.ch.huji.ac.il

Abstract: The active species, Compound I, of horseradish peroxidase (HRP) has been investigated by quantum mechanical/molecular mechanical (QM/MM) calculations using 10 different QM regions. In accord with experimental data, the lowest doublet and quartet states are found to be virtually degenerate, with two unpaired electrons on the FeO moiety and one localized on the porphyrin in an a_{2u}-dominant orbital with a minor, but nonnegligible, a_{1u} component. The proximal ligand appears to be imidazole rather than imidazolate. The hydrogen-bonding network around the FeO moiety (i.e., Arg_{38} and His_{42}) has significant influence on the axial bonds and the spin density distribution in the FeO moiety. Including this network in the QM region was found to be essential for reproducing the experimental Mössbauer parameters. The protein environment shapes most of the subtle features of Compound I of HRP.

I. Introduction

Heme peroxidases constitute an important group of enzymes that are widespread in nature and found in plants, fungi, bacteria, and mammals.[1,2] These enzymes utilize hydrogen peroxide to oxidize organic compounds and thereby perform physiological functions, such as elimination of byproducts of aerobic respiration, synthesis of cell wall components, and metabolism of hormones. Among the peroxidases, horseradish peroxidase (HRP)[3] is the most widely studied enzyme that has played an important role in the history of modern enzymology.[1,4] The main function of HRP appears to be the oxidation of phenols which subsequently polymerize and serve to build and repair the cell walls in higher plants.[3b]

All peroxidases possess a heme (protoheme IX), Scheme 1, and with the exception of chloroperoxidase,[1,2b] the heme is held in the proximal side by an imidazole ring of a histidine (His) side chain of the encapsulating protein. The enzymes share the same catalytic cycle, shown in Scheme 1. The resting state reacts with hydrogen peroxide[2b] to yield the primary active species of the enzyme, known as Compound I (Cpd I).[1,2] Cpd I abstracts an electron from a substrate, S−H, and thereby gets converted to a secondary species, so-called Compound II (Cpd II),[5] which in turn, oxidizes another molecule of substrate and regenerates the resting state. Cpd I and Cpd II store, respectively, two and one oxidation equivalents, above the resting state, and contain high-valence iron in oxo-ferryl moieties, which are responsible for the oxidative function of the enzyme. Cpd I is the primary oxidant of heme peroxidases and has therefore been studied thoroughly. It is also the target of the present paper that

[†] The Hebrew University of Jerusalem.
[‡] Max-Planck-Institut für Kohlenforschung.

(1) For a monograph on heme peroxidases, see: Dunford, H. B. *Heme Peroxidases*; Wiley-VCH: New York, 1999.

(2) For general reviews on heme peroxidases, see: (a) In *Handbook of Metalloproteins*; Messerschmidt, A., Huber, R., Poulos, T. L., Wieghardt, K., Eds.; John-Wiley and Sons: NY, 2001, Vol. 1, pp 193−328. (b) Poulos, T. L. Peroxidases and Cytochrome P450. In *The Porphyrin Handbook*; Kadish, K. M., Smith, K. M., Guilard, R., Eds.; Academic Press: 2000; Vol. 4, Chapter 32, pp 189−218. (c) Dawson, J. H. *Science* **1988**, *240*, 433−439. (d) Dawson, J. H.; Sono, M. *Chem. Rev.* **1987**, *87*, 1255−1276. (e) Marnett, L. J.; Kennedy, T. A. Comparison of Peroxidase Activity of Hemoprotein and Cytochrome P450. In *Cytochrome P450: Structure, Mechanisms and Biochemistry*, 2nd ed.; Ortiz de Montellano, P. R., Ed.; Plenum Press: NY, 1995; pp 49−80. (f) Poulos, T. L., Cupp-Vickery, J., Li, H. Structural Studies on Prokaryotic Cytochromes P450. In *Cytochrome P450: Structure, Mechanisms and Biochemistry*, 2nd ed.; Ortiz de Montellano, P. R., Ed.; Plenum Press: New York, 1995; Chapter 4, pp 125−150. (g) Meunier, B. Models of Heme Peroxidases and Catalases. In *Biomimetic Oxidations Catalyzed by Transition Metal Complexes*; Meunier, B., Ed.; Imperial College Press: UK, 2000; Chapter 4, pp 171−214. (h) Meunier, B. *Chem. Rev.* **1992**, *92*, 1411−1456. (i) Watanabe, Y. High-Valent Intermediates. In *The Porphyrin Handbook*; Kadish, K. M., Smith, K. M., Guilard, R., Eds.; Academic Press: 2000; Vol. 4, Chapter 30, pp 97−118. (j) Poulos, T. L. *J. Biol. Inorg. Chem.* **1996**, *1*, 356−359.

(3) For HRP structures, see: (a) Gajhede, M.; Schuller, D. J.; Henriksen, A.; Smith, A. T.; Poulos, T. L. *Nat. Struct. Biol.* **1997**, *4*, 1032−1038. (b) Gajhede, M. Horseradish Peroxidase. In *Handbook of Metalloproteins*; Messerschmidt, A., Huber, R., Poulos, T. L., Wieghardt, K., Eds.; John-Wiley and Sons: New York, 2001; Vol. 1, pp 195−210. (c) Hiner, A. N. P.; Raven, E. L.; Thorneley, R. N. F.; Garcia-Canovas, F.; Rodriguez-Lopez, J. N. *J. Inorg. Biochem.* **2002**, *91*, 27−34.

(4) (a) For the discovery of Planchet in 1810 that horseradish roots change the color of an alcoholic tincture of guaiac resin, when exposed to hydrogen peroxide, see: Frouton, J. S. *Molecules and Life: Historical Essays of Chemistry and Biology*; Wiley-Interscience: 1972. (b) For the controversy of Wiltstäter (who purified HRP and was familiar with heme chemistry) and Sumner (who crystallized jack bean urease) on whether the catalytic effect of the enzyme is an intrinsic property of the protein or a property of trace inorganic contaminant, see pages 4−5 in ref 1.

(5) Cpd II is either an Fe^{IV}═O or Fe^{IV}OH species. For example, see: (a) EXAFS of Cpd I and Cpd II: Penner-Han, J.; McMurry, T.; Renner, M.; Latos-Grazynsky, L.; Elbe, K. S.; Davis, I. M.; Balch, A. L.; Groves, J. T.; Dawson, H. K. *J. Biol. Chem.* **1983**, *258*, 12761−12764. (b) Cpd II of chloroperoxidase: Green, M. T.; Dawson, J. D.; Gray, H. B. *Science* **2004**, *304*, 1653−1656. (c) Rovira, C. *Chem. Phys. Chem.*, **2005**, *6*, 1−8.

Scheme 1 Catalytic Cycle of Peroxidases

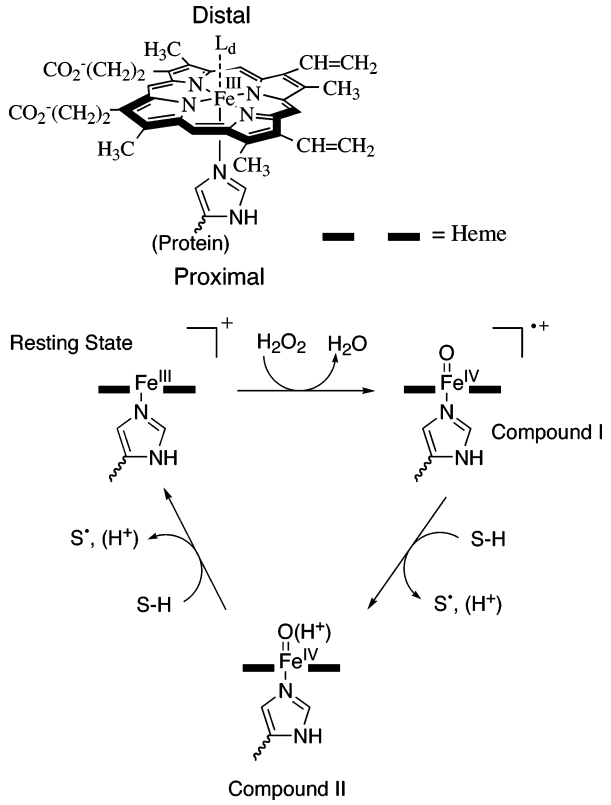

investigates the structure and properties of Cpd I of HRP by means of quantum mechanical/molecular mechanical (QM/MM) calculations.

Cpd I of HRP was discovered by Theorell,[6a] who first prepared Cpd I as a green compound that rapidly changed to a red species (later identified as Cpd II). Cpd I and Cpd II were distinguished by kinetic measurements of Chance[6b] and George.[6c] George showed that Cpd II has a ferryl group (Fe^{IV}), postulated that Cpd I has iron in a higher oxidation state, Fe^{V}, and basically outlined the catalytic cycle as is currently accepted. Subsequently, other techniques were used to investigate electronic and structural features of Cpd I. The molecular dimensions of Cpd I were determined by EXAFS,[5a,7] and recently X-ray crystallography,[8] both exhibiting a short FeO bond, 1.64−1.70 Å, with double bond character. Some features of the proximal and distal sides of the heme in the X-ray structures of HRP species[2b,3a,8] are shared by many of the peroxidases (see Figure 1). The distal side has a highly conserved histidine (His_{42}) and arginine (Arg_{38}), which are bridged by a molecule of water (W_{427}). These groups are thought to constitute the proton relay machinery that converts the resting state and hydrogen peroxide to Cpd I + H_2O.[2b,c,j] Being rather close to the oxo-iron moiety, these groups might also influence the properties of Cpd I. The proximal side has a highly conserved aspartate, Asp_{247}, which is in a hydrogen bonding distance from the N−H group of the proximal ligand, His_{170}, and a phenylalanine, Phe_{221}, that stacks with the imidazole ring of His_{170} via $\pi-\pi$ interactions.[2b,3a] In addition, the two propionate side chains on the protoporphyrin IX ring are held by salt bridges with Arg_{31} and Gln_{76}, and by H-bonds with Ser_{35}, Ser_{73}, and water molecules (W_{278}, W_{423}). These groups are also close to the central moieties of Cpd I and may affect its features.

Despite the extensive knowledge that exists on HRP Cpd I, there are still uncertainties concerning the electronic structure of this species. This was probed for the first time by means of Mössbauer spectroscopy, which revealed an iron(IV) ion,[9] and later by EPR and electronic spectra of model compounds, which suggested that Cpd I must contain a porphyrin radical cationic state,[10] with one electron in an a_{1u} or a_{2u} orbital.[10c] These pioneering studies were extended later using a variety of techniques, including Mössbauer, EPR/ENDOR, NMR, and resonance Raman spectroscopies.[11−13] A combination of ^{17}O ENDOR and ^{14}N ENDOR experiments[11c,d] identified the ground state as having a triplet spin pair on the Fe^{IV}═O unit coupled to a doublet spin on the porphyrin ring that is present as a radical cationic species (i.e., $Fe^{IV}OPor^{+\bullet}$). Since strong resonances appeared on the pyrrole nitrogen atoms of the porphyrin, the ground state was assigned as an A_{2u} state, in which the odd electron resides in the a_{2u} orbital of the porphyrin moiety. Mössbauer spectra[11h] support the assignment of spin coupling between an oxo-iron triplet and a porphyrin cation radical. The resonance Raman spectra of Cpd I of HRP have been interpreted in terms of an A_{1u} ground state[13a] and an A_{2u} ground state.[13b] At present, the A_{2u} assignment appears to be the consensus among the experimentalists in the field. What seems to be less established is the total spin quantum number of the ground state due to the three unpaired electrons on the FeO and porphyrin moieties (Scheme 2), which can couple ferromagnetically as in Scheme 2a, or antiferromagnetically as in Scheme 2b. Magnetic susceptibility measurements suggest a quartet state with ferromagnetic coupling,[14] while EPR spectroscopy seems to favor an antiferromagnetic state (part of a Kramers doublet),[11e,g] with an extremely small coupling of the porphyrin radical to the triplet electrons in the Fe^{IV}═O moiety. Modeling of EPR

(6) (a) Theorell, H. *Enzymologia* **1941**, *10*, 250−252. (b) Chance, B. *Arch. Biochem.* **1949**, *24*, 389−409. (c) George, P. *Biochem. J.* **1953**, *55*, 220−230.
(7) (a) Chance, B.; Powers, L.; Ching, Y.; Poulos, T.; Schonbaum, G. R.; Yamazaki, I.; Paul, K. G. *Arch. Biochem. Biophys.* **1984**, *235*, 596−611. (b) Chance, M.; Powers, L.; Poulos, T.; Chance, B. *Biochemistry* **1986**, *25*, 1266−1270.
(8) Berglund, G. I.; Carlsson, G. H.; Smith, A. T.; Szoeke, H.; Henriksen, A.; Hajdu, J. *Nature* **2002**, *417*, 463−468.
(9) Moss, T. H.; Ehrenberg, A.; Bearden, A. J. *Biochemistry* **1969**, *8*, 4159−4162.
(10) (a) Dolphin, D.; Forman, A.; Borg, D. C.; Fajer, J.; Felton, R. H. *Proc. Natl. Acad. Sci. U.S.A.* **1971**, *68*, 614−618. (b) Dolphin, D.; Felton, R. H. *Acc. Chem. Res.* **1974**, *7*, 26−32. (c) DiNello, R. K.; Dolphin, D. H. *J. Biol. Chem.* **1981**, *256*, 6903−6912.
(11) EPR and ENDOR data: (a) Asa, R.; Vönngård, T.; Dunford, H. B. *Biochim. Biophys. Acta* **1975**, *391*, 259−263. (b) Schultz, C. E.; Devaney, P. W.; Winkler, H.; Debrunner, P. G.; Doan, N.; Chiang, R.; Rutter, R.; Hager, L. P. *FEBS Lett.* **1979**, *103*, 102−105. (c) Roberts, J. E.; Hoffman, B. M.; Rutter, R.; Hager, L. P. *J. Biol. Chem.* **1981**, *256*, 2118−2121. (d) Roberts, J. E.; Hoffman, B. M.; Rutter, R.; Hager, L. P. *J. Am. Chem. Soc.* **1981**, *103*, 7654−7656. (e) Rutter, R.; Valentine, M.; Hendrich, M. P.; Hager, L. P.; Debrunner, P. G. *Biochemistry* **1983**, *22*, 4769−4774. (f) Rodriguez-Lopez, J. N.; Lowe, D. J.; Hernandez-Ruiz, J.; Hiner, A. N. P.; Garcia-Canovas, F.; Thorneley, R. N. F. *J. Am. Chem. Soc.* **2001**, *123*, 11838−11847. (g) Weiss, R.; Mandon, D.; Wolter, T.; Trautwein, A. X.; Müther, M.; Bill, E.; Gold, A.; Jayaraj, K.; Terner, J. *J. Biol. Inorg. Chem.* **1996**, *1*, 377−383. (h) For Mössbauer and EPR analyses, see: Schulz, C. E.; Rutter, R.; Sage, J. T.; Debrunner, P. G.; Hager, L. P. *Biochemistry* **1984**, *23*, 4743−4754.
(12) For NMR data, see: (a) La Mar, G. N.; de Ropp, J. S.; Smith, K. M.; Langry, K. C. *J. Biol. Chem.* **1981**, *256*, 237−243. (b) Thanabal, V.; La Mar, G. N.; De Ropp, J. S. *Biochemistry* **1988**, *27*, 5400−5407. (c) de Ropp, J. S.; Sham, S.; Asokan, A.; Newmyer, S.; Ortiz de Montellano, P. R.; La Mar, G. N. *J. Am. Chem. Soc.* **2002**, *124*, 11029−11037.
(13) For resonance Raman assignments, see: (a) Kincaid, J. R.; Zheng, Y.; Al-Mustafa, J.; Czarnecki, K. *J. Biol. Chem.* **1996**, *271*, 28805−28811. (b) Chuang, W. J.; Van Wart, H. E. *J. Biol. Chem.* **1992**, *267*, 13293−13301.
(14) Theorell, H.; Ehrenberg, A. *Arch. Biochem. Biophys.* **1952**, *41*, 442−461.

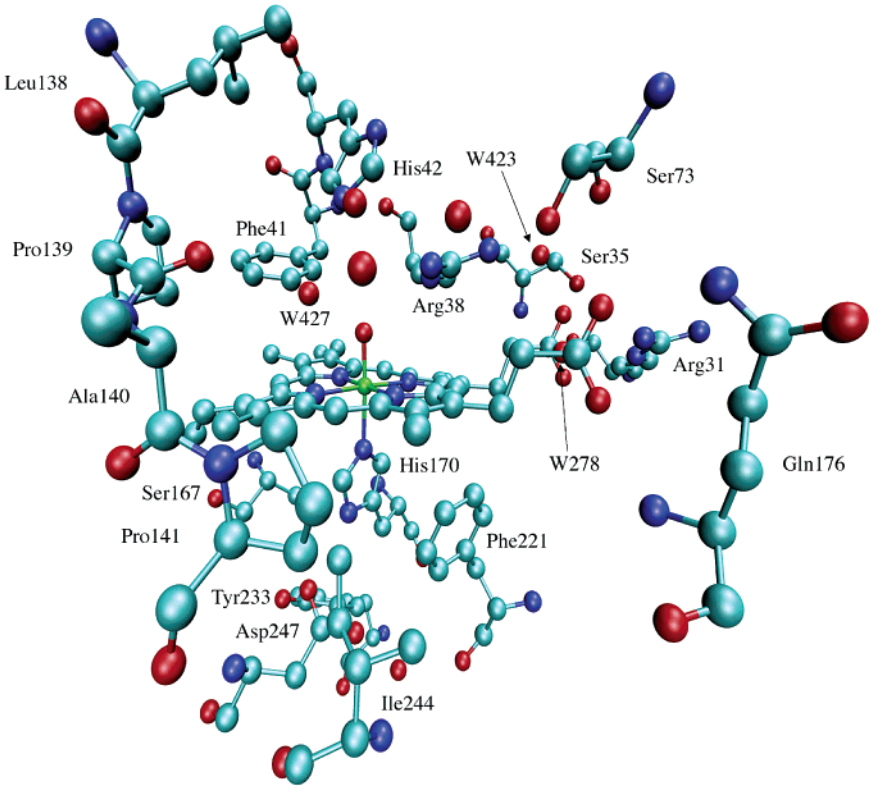

Figure 1. A view of the active site of HRP (PDB code: 1HCH). Residues are labeled according to this PDB file (hydrogen atoms are not shown).

Scheme 2. (a) Ferromagnetic and (b) Antiferromagnetic Coupling in the Ground State of Cpd I[a]

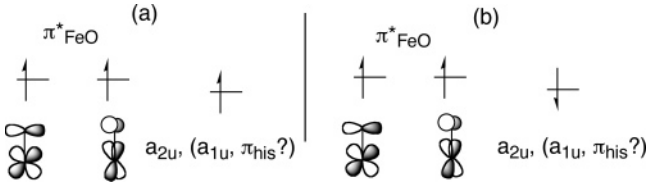

[a] The identity of the third orbital is in question. The term symbol of the ground state carries the label of the third orbital, e.g., A_{2u} if the orbital is a_{2u}.

spectra[11h] suggests that the ground state is a mixture of ferromagnetically and antiferromagnetically coupled states.

Whereas EPR, Mössbauer, and resonance Raman studies all place the radical exclusively on the porphyrin ring, NMR data (nuclear overhauser effect, NOE)[12] indicate a significant π-radical character on the proximal histidine ligand, which is the reason for the question mark on the identity of the third orbital in Scheme 2. This character might be induced by the hydrogen bond to the aspartate (Figure 1) endowing the histidine with imidazolate-like features,[12b] or by complete deprotonation of the N−H moiety, resulting in a histidinate (imidazolate) proximal ligand.

Cpd I species of HRP and other peroxidases have been the subject of theoretical studies, which utilized simplified models of the active species without the surrounding protein.[15] The earlier treatments were carried out with semiempirical methods (iterative extended Hückel and INDO) and were nonuniform in their conclusions.[16] One study[16a] calculated the Mössbauer parameters and assigned the ground state of Cpd I HRP as the ferromagnetic $^4A_{2u}$ state with $S = {}^3/_2$. The other two studies[16b,c] assigned the ground state as A_{1u} and showed that only an imidazolate representation of the ligand can reproduce: (i) the observed[3b] reduction of the intensity in the Soret band of Cpd I vis-à-vis the resting state and (ii) the NMR contact-shift data[12] that implies delocalization of the radical to the imidazole ligand. By contrast, all recent studies that were carried out by density functional theory (DFT)[15,17] assigned the ground state as A_{2u}, generally, but not always,[17c] with ferromagnetic coupling, namely $^4A_{2u}$ ($S = {}^3/_2$). In most studies which involve geometry optimization, the coupling between the electron on the porphyrin and the triplet pair on the Fe^{IV}=O moiety was computed to be rather large, 50−80 cm^{-1} or more. Smaller couplings were obtained when more residues besides the active species were included in the calculation[17c] or when imidazolate was used to represent the proximal ligand.[17b] In the latter case, the ligand was found to carry a major fraction of the spin density (ca. 80%),[17b] thus lending support to the conclusion from the NMR studies about the delocalization of the radical species to the proximal ligand.[12] By contrast, when incorporating the highly conserved Asp_{247} into the DFT calculations,[17c,18] and accounting for the polarization of the species by the environment,[17c] the N−H bond of the imidazole remained intact and no spin density

(15) For reviews of theoretical studies, see: (a) Harris, D. L. *Curr. Opin. Chem. Biol.* **2001**, *5*, 724−735. (b) Harris, D. L.; Loew, G. H. *J. Porphyrins Phthalocyanins* **2001**, *5*, 334−344.

(16) (a) Loew, G. H.; Kert, C. J.; Hjelmeland, L. M.; Kirchner, R. F. *J. Am. Chem. Soc.* **1977**, *99*, 3534−3536. (b) Du, P.; Loew, G. H. *Biophys. J.* **1995**, *68*, 69−80. (c) Loew, G. H.; Axe, F. U.; Collins, J. R.; Du, P. *Inorg. Chem.* **1991**, *30*, 2291−2294.

(17) (a) Deeth, R. J. *J. Am. Chem. Soc.* **1999**, *121*, 6074−6075. (b) Green, M. T. *J. Am. Chem. Soc.* **2000**, *122*, 9495−9499. (c) de Visser, S. P.; Shaik, S.; Sharma, P. K.; Kumar, D.; Thiel, W. *J. Am. Chem. Soc.* **2003**, *125*, 15779−15788. (d) Kuramochi, H.; Noodleman, L.; Case, D. A. *J. Am. Chem. Soc.* **1997**, *119*, 11442−11451. (e) Rydberg, P.; Sigfridsson, E.; Ryde, U. *J. Biol. Inorg. Chem.* **2004**, *9*, 203−223. (f) Antony, J.; Grodzicki, M.; Trautwein, A. X. *J. Phys. Chem. A* **1997**, *101*, 2692−2701.

(18) DFT calculations of Cpd I of CcP with Asp and Trp residues in the proximal side: Wirstam, M.; Blomberg, M. R. A.; Siegbahn, P. E. M. *J. Am. Chem. Soc.* **1999**, *121*, 10178−10185.

accumulated on the imidazole ligand. An early ab initio study with a minimal basis set and inclusion of polarization by protein residues indicated that the imidazolate/Asp−H representation of the ligand may be preferred over the imidazole/Asp$^-$ tautomer.[19] A more recent[15b] study employing DFT (BPW91) for electronic structure determination and INDO/S/CI for spectra showed that the imidazolate/Asp−H and imidazole/Asp$^-$ tautomers differ in energy by no more than 1 kcal/mol, but *only the first representation could reproduce the observed shift in* the Soret band of HRP Cpd I vs that of chloroperoxidase Cpd I.

Clearly, the nature of HRP Cpd I involves a few unresolved issues, concerning the A_{2u} nature of the ground state, its spin quantum number, and the protonation state of its proximal ligand. One hopes that theory can clarify these issues, but experience has shown[15a,17c] that these questions are too *subtle* to be safely tackled by calculations on simplified models. The QM/MM method offers to-date potentially the best theoretical tool to resolve such problems, since it computes the active species within its native protein, thus accounting for the possible chemical influence of the neighboring residues, as well as of the polarity, hydrogen bonding capability, and steric constraints of the protein. Previous experience with Cpd I of cytochrome P450 reveals that QM/MM calculations can be useful for similar problems if care is taken to include in the QM region all the relevant residues for a given problem.[20,21] Thus, the QM/MM models, in this study, will evolve gradually to include suitable representations of all residues in the proximal and distal sides of the heme that are shown in Figure 1. In addition, we shall explore the imidazolate character of the proximal ligand by employing a full QM/MM scan between the two tautomeric forms, Im−H/Asp$^-$ and Im$^-$/Asp−H. In view of the postulated role of the propionate side chains as a potential conduit for the electron-transfer process to Cpd I,[22] and computational findings[23] that there is significant delocalization of the odd electron density from the porphyrin to the propionates in P450 Cpd I, we shall address this issue as well.

II. Methods

A. QM/MM Methodology and Software. The QM/MM method[24] dissects the total enzyme into two subsystems: the active center and the rest. The active center is described by a quantum mechanical method, in the present case DFT in the unrestricted Kohn−Sham formalism employing the B3LYP functional.[25] The rest of the system (see below) is treated by molecular mechanics using a force field calibrated for proteins.[20,26] The two subsystems are allowed to interact by electrostatic and van der Waals terms, such that the QM subsystem adapts its electronic structure and charge distribution to the field exerted by the protein environment. In the present study we apply the electrostatic embedding scheme[27] that incorporates the MM charges into the one-electron Hamiltonian of the QM procedure, while the dangling bonds at the QM/MM boundary are capped with hydrogen link atoms[28] in the framework of the charge shift method.[28f] The Chemshell software[29] is used to perform the QM/MM calculations by integrating the TURBOMOLE package[30] for QM and the DL-POLY program[31] for MM using the CHARMM22 force field.[26]

Two basis sets were employed in this study: the first one (B1) for geometry optimization and the second (B2) for single-point energy calculations. These single-point results are abbreviated as B2//B1. B1 consists of an effective core potential on iron with the associated double ζ basis set LACVP[32] and the 6-31G basis set[33] on all other atoms. In B2, iron is described by Wachters' all-electron basis set augmented with diffuse d and f polarization functions,[34] while the immediate coordination sphere of iron and other electronegative atoms are represented by 6-31+G(d), and the remaining atoms by 6-31G(d).

B. Setup of the System. To prepare suitable initial structures for the QM/MM calculations, we started from the experimental X-ray structure of HRP Cpd I (PDB code: 1HCH)[8] and built a complete model of the solvated enzyme by adding the missing hydrogen atoms and a 16-Å-thick water solvent layer. The complete system consists of 19 452 atoms, including 13 395 atoms in the solvent. The system was relaxed by performing pure force field energy minimizations and short molecular dynamics (MD) simulations, using the CHARMM22 force field.[26] During these classical force field calculations, the coordinates of the entire heme unit and the coordinating histidine were kept fixed. The MD calculations did not significantly modify the structure compared with the initial X-ray structure. Therefore, we performed the QM/MM calculations on the coordinates obtained after simple force field energy minimizations and short MD on the inner solvent layer (in order to remove close contacts) and not on the coordinates that were obtained after equilibration by long MD simulations.

C. Definition of the QM Regions. Schemes 3 and 4 depict the different models of the QM subsystem that were used in this study to describe the active center. These models are numbered as **1** to **10**. The simplest QM region, **1**, consists of an oxo-iron porphine and an imidazole (ImH) as a sixth ligand. Subsequent models were enlarged gradually to include the key residues, which have hydrogen bonds with the proximal ligand, with the propionate side chains, and with the distal side of the macrocycle.

QM regions **2**−**4** include the hydrogen-bonding network around the proximal histidine ligand. **2** contains a formate ion, which mimics the

(19) Menyhard, D. K.; Naray-Szabo, G. *J. Phys. Chem. B* **1999**, *103*, 227−233.
(20) (a) Schöneboom, J. C.; Lin, H.; Reuter, N.; Thiel, W.; Cohen, S.; Ogliaro, F.; Shaik, S. *J. Am. Chem. Soc.* **2002**, *124*, 8142−8151. (b) Schöneboom, J. C.; Cohen, S.; Lin, H.; Shaik, S.; Thiel, W. *J. Am. Chem. Soc.* **2004**, *126*, 4017−4034. (c) Schöneboom, J. C.; Thiel, W. *J. Phys. Chem. B* **2004**, *108*, 7468−7478. (d) Altun, A.; Thiel, W. *J. Phys. Chem. B* **2005**, *109*, 1268−1280. (e) Schöneboom, J. C.; Neese, F.; Thiel, W. *J. Am. Chem. Soc.* **2005**, *127*, 5840−5853.
(21) Shaik, S.; Kumar, D.; de Visser, S. P.; Altun, A.; Thiel, W. *Chem. Rev.* **2005**, *105*, 2279−3935.
(22) Sundaramoorthy, M.; Kishi, K.; Gold, M.; Poulos, T. *J. Biol. Chem.* **1994**, *269*, 32759−32767.
(23) Guallar, V.; Friesner, R. A. *J. Am. Chem. Soc.* **2004**, *126*, 8501−8508.
(24) For some reviews, see: (a) Aqvist, J.; Warshel, A. *Chem. Rev.* **1993**, *93*, 2523−2544. (b) Gao, J. In *Reviews in Computational Chemistry*; Lipkowitz, K. B., Boyd, D. B., Eds.; VCH: Weinheim, 1995; Vol. 7, p 119. (c) Mordasini, T. Z.; Thiel, W. *Chimia* **1998**, *52*, 288−291. (d) Monard, G.; Merz, K. M., Jr. *Acc. Chem. Res.* **1999**, *32*, 904−911. (e) Sherwood, P. In *Modern Methods and Algorithms of Quantum Chemistry*; Grotendorst, J., Ed.; NIC Series 3; John von Neumann Institute for Computing: Jülich, 2000; p 285. (f) Gao, J.; Truhlar, D. G. *Annu. Rev. Phys. Chem.* **2002**, *53*, 467−505. (g) Field, M. J. *J. Comput. Chem.* **2002**, *23*, 48−58. (h) Monard, G.; Prat-Resina, X.; Gonzalez-Lafont, A.; Lluch, J. M. *Int. J. Quantum Chem.* **2003**, *93*, 229−244. (i) Ridder, L.; Mulholland, A. *Curr. Top. Med. Chem.* **2003**, *3*, 1241−1256.
(25) (a) Becke, A. D. *Phys. Rev. A* **1988**, *36*, 3098−3100. (b) Lee, C.; Yang, W.; Parr, R. G. *Phys. Rev. B* **1988**, *37*, 785−789. (c) Becke, A. D. *J. Chem. Phys.* **1993**, *98*, 5648−5652.
(26) MacKerell, A. D., Jr. et al. *J. Phys. Chem. B* **1998**, *102*, 3586−3616.
(27) Bakowies, D.; Thiel, W. *J. Phys. Chem.* **1996**, *100*, 10580−10594.
(28) (a) Field, M. J.; Bash, P. A.; Karplus, M. *J. Comput. Chem.* **1990**, *11*, 700−733. (b) Amara, P.; Field, M. J. *Theor. Chem. Acc.* **2003**, *109*, 43−52. (c) Reuter, N.; Dejaegere, A.; Maigret, B.; Karplus, M. *J. Phys. Chem. A* **2000**, *104*, 1720−1735. (d) Singh, U. C.; Kollman, P. A. *J. Comput. Chem.* **1986**, *7*, 718−730. (e) Derat, E.; Bouquant, J.; Humbel, S. *THEOCHEM* **2003**, *632*, 61−69. (f) de Vries, A. H.; Sherwood, P.; Collins, S. J.; Rigby, A. M.; Rigutto, M.; Kramer, G. J. *J. Phys. Chem. B* **1999**, *103*, 6133−6141.
(29) Sherwood, P. et al. *THEOCHEM* **2003**, *632*, 1−28.
(30) Ahlrichs, R.; Bär, M.; Häser, M.; Horn, H.; Kölmel, C. *Chem. Phys. Lett.* **1989**, *162*, 165−169.
(31) Smith, W.; Forester, T. *J. Mol. Graph.* **1996**, *14*, 136−141.
(32) (a) Hay, J. P.; Wadt, W. R. *J. Chem. Phys.* **1985**, *82*, 299−310. (b) Friesner, R. A.; Murphy, R. B.; Beachy, M. D.; Ringlanda, M. N.; Pollard, W. T.; Dunietz, B. D.; Cao, Y. X. *J. Phys. Chem. A* **1999**, *103*, 1913−1928.
(33) Hehre, W. J.; Ditchfield, R.; Pople, J. A. *J. Chem. Phys.* **1972**, *56*, 2257−2261.
(34) Wachters, A. J. H. *J. Chem. Phys.* **1970**, *52*, 1033−1036.

Scheme 3. QM Regions 1−9 Used in the QM/MM Study

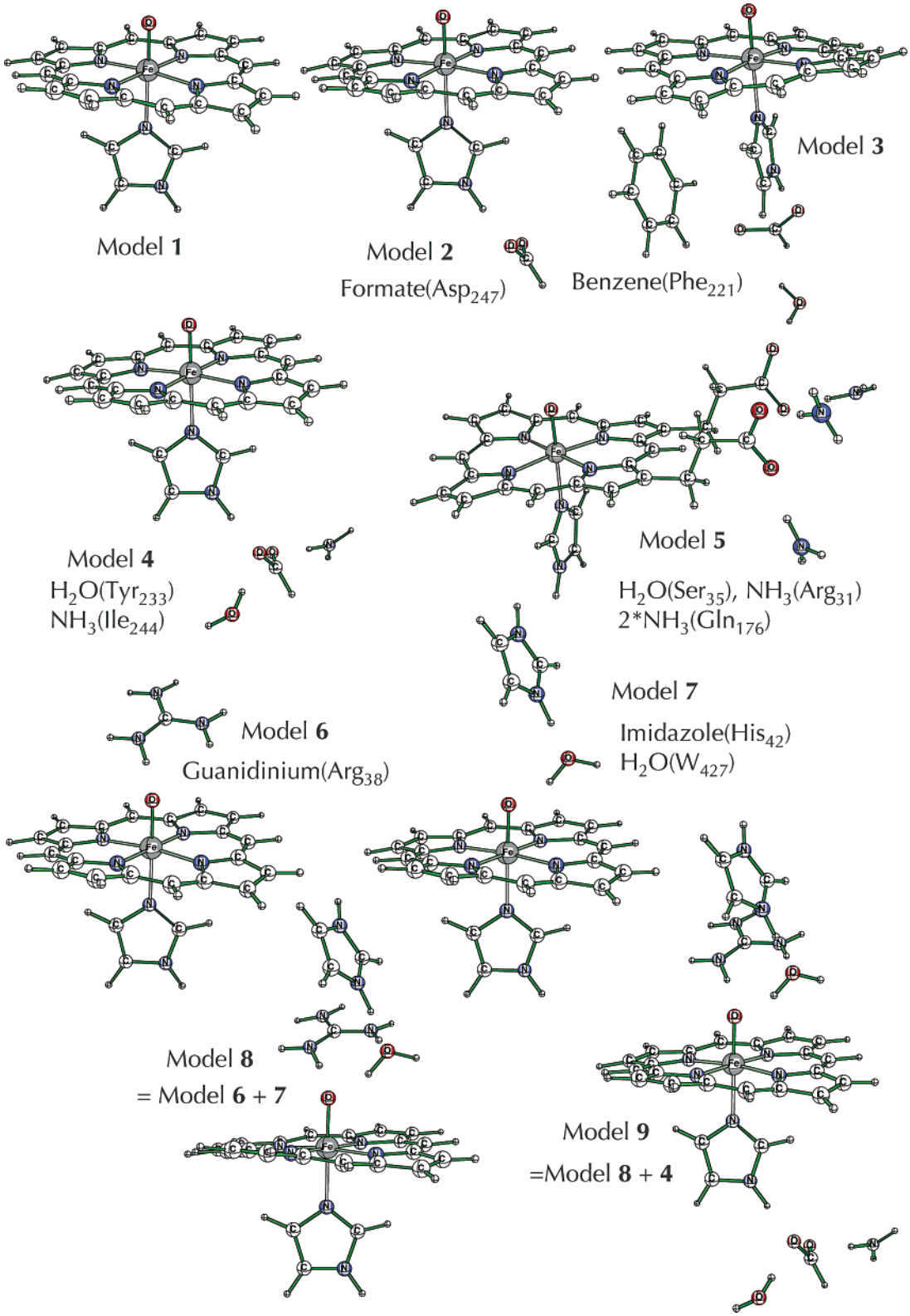

interaction of the side chain of Asp_{247} with the histidine connected to iron. In **3**, a benzene molecule is added to represent the side chain of the Phe_{221} residue. Since, in the crystal structure, the carboxylate group of the side chain of Asp_{247} appears to be connected by hydrogen bonds not only to histidine but also to Tyr_{233} and Ile_{244}, we included these hydrogen bonds in **4**, using HO(H) to model the side chain of Tyr_{233} and $NH_2(H)$ to model the side chain of Ile_{244}; the atoms in parentheses indicate the hydrogen link atom.

QM region **5** involves the lateral propionate chains of the heme. In addition to the two propionates, it contains models for the residues that interact with the propionates by salt bridges and/or hydrogen bonding; these residues are Ser_{35}, Arg_{31}, and Gln_{176}, which are modeled as HO(H), $NH_2(H)$, and two units of $NH_2(H)$, respectively. The use of $NH_2(H)$ to represent Arg_{31} reflects the interaction of a single NH_2 unit with the propionate, but since it lacks the positive charge of the arginine, this representative may underestimate the screening power of Arg_{31}.

Scheme 4. QM Region 10 Used in the QM/MM Study (See Text).

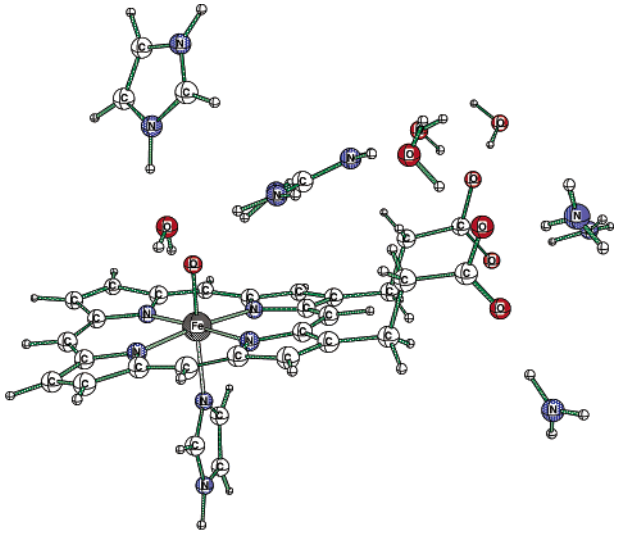

Gln_{176} donates two NH- - -O hydrogen bonds to the carboxylic group of the propionate (one from the side chain NH, the other from the backbone NH) and is therefore modeled by two $NH_2(H)$ units.

QM regions **6**−**8** in Scheme 3 account for the interaction of the protein environment with the oxo group of Cpd I in the distal side. **6** involves only Arg_{38} (here represented by a guanidinium group since it interacts by cyclic H-bonding with a water molecule and the oxo-iron moiety). Another key residue in the vicinity of the heme group is His_{42}, which is included in **7** as an imidazole, together with a bridging water molecule that has a hydrogen bond to the oxo-iron. **8** is the sum of **6** and **7**, hence including Arg_{38}, His_{42}, and the bridging water molecule. **9** combines the networks of hydrogen bonds in the distal and proximal sides. Finally, QM region **10** (see Scheme 4) includes the propionate side chains, Arg_{38}, His_{42}, and the bridging water, accounting for the fact that Arg_{38} is connected by two water molecules to the propionate side chains.

D. Protonation State of the Proximal Ligand. As stated in the Introduction, NMR evidence suggests significant spin density on the imidazole proximal ligand, thereby suggesting at least partial imidazolate character.[12] Thus, the proximal ligand may involve either imidazole/aspartate anion or imidazolate/aspartic acid. To resolve this issue, we performed QM/MM potential energy surface (PES) scans for the proton transfer from Asp_{247} to His_{170} (initially deprotonated) using QM region **4**. This was done by fully relaxing all degrees of freedom along the proton transfer coordinate (the starting point is fully optimized).

E. Mössbauer Parameters. Since Mössbauer spectra are available in the literature, it is possible to compare Mössbauer parameters obtained by theoretical means with the experimental values. Using the ORCA program,[35] the Mössbauer parameters were obtained from single-point B3LYP calculations (at the geometries obtained after QM/MM optimization). The isomer shift was evaluated from the electron density at the iron nucleus.[36] Iron was described by the triply polarized core properties basis set CP(PPP)[36] and the other atoms by the SV(P) basis set[37] with the inner s-functions left uncontracted. For the iron atom, an enhanced integration grid was used, and the overall integration accuracy was increased to 7.[36] MM point charges were included in these calculations to probe the effect of the protein environment. To ascertain the influence of neighboring residues on the Mössbauer parameters, the calculations were performed for QM regions **1** and **8**.

(35) Neese, F. *ORCA*, version 2.4, revision 10; Max-Planck-Institut für Bioanorganische Chemie: Mülheim a. d. Ruhr, Germany, 2004.
(36) Neese, F. *Inorg. Chim. Acta* **2002**, *337*, 181−192.
(37) Schäfer, A.; Horn, H.; Ahlrichs, R. *J. Chem. Phys.* **1992**, *97*, 2571−2577.

Table 1. Relative B3LYP/CHARMM Spin State Energies (^{2}A−^{4}A) in kcal/mol for Models **1**−**10** of HRP Cpd I[a]

model	B1, MM Opt.[b]	B1, QM/MM Opt.[c]	B2, single point[d]
1	0.13	−0.07	−0.23
2	0.10	0.06	0.20
3	0.24	−0.07	−0.41
4	0.13	−0.04	−0.36
5	0.16	0.00	−0.24
6	0.07	0.03	0.05
7	0.14	−0.14	−0.19
8	0.08	−0.13	−0.05
9	−0.17	−0.11	−0.08
10	0.08	−0.11	−0.01

[a] A positive value means the quartet state is more stable. [b] Single-point QM/MM calculations at the CHARMM-minimized X-ray structure keeping the coordinates of the entire heme and the coordinating histidine similar to the X-ray conformation (before performing any QM/MM optimization). [c] From individual QM/MM geometry optimizations for the doublet and quartet states of each model. [d] Single-point QM/MM calculations (B2//B1) at the QM/MM-optimized structures.

III. Results

Detailed numerical results are summarized in the Supporting Information. In the following we focus on the key results.

A. Relative Spin State Energies. By applying the methodology described above, we computed the energy differences between the doublet (^{2}A) and quartet (^{4}A) states of HRP Cpd I. The results for models **1**−**10** with different QM regions are summarized in Table 1, where a positive (negative) value implies a quartet (doublet) ground state. The first column lists QM(B3LYP/B1)/MM energy differences at a common geometry obtained from the PDB coordinates and subsequent CHARMM minimization (see Section II.B): with this setup, the quartet is the ground state for all models except **9**, but the two spin states are always close in energy (maximum splitting of 0.24 kcal/mol for **3**). Individual QM(B3LYP/B1)/MM geometry optimizations for all models and states reverse this trend and generally yield a doublet ground state (except for **2** and **6**), but the doublet-quartet splittings remain small (maximum of 0.14 kcal/mol for **7**). Single-point energy evaluations (B2//B1) at these QM/MM-optimized geometries using the larger B2 basis confirm the preference for a doublet ground state, again with exception of **2** and **6** (maximum splitting of 0.41 kcal/mol for **3**).

For the largest model **10**, the doublet state is below the quartet state by 5 cm^{-1} (B2//B1); the experimental values range from +2 to −2 cm^{-1}.[11g,h] The energy differences in Table 1 have not been corrected for zero-point energies (ZPE) which are expected to be very similar in the two spin states. This has been confirmed for the smallest model **1** by computing the harmonic frequencies of the QM region via finite differences of the QM/MM gradient: the resulting estimate of the ZPE correction to the doublet-quartet gap is 0.11 kcal/mol.

B. Geometries. The QM/MM optimization changes the gas-phase geometry of the QM regions. Some global changes are depicted in Figure 2. Thus, relative to the gas phase,[17c] the QM/MM structure shows a slight rotation of the imidazole (by 12°) and puckering of the porphine plane. These global changes are associated with some bond length and angular variations. The cartesian coordinates of all the models are documented in the Supporting Information; while in what follows we discuss only the important points.

Some key geometric parameters are summarized in Table 2. These are the distances between the iron and the oxygen of the

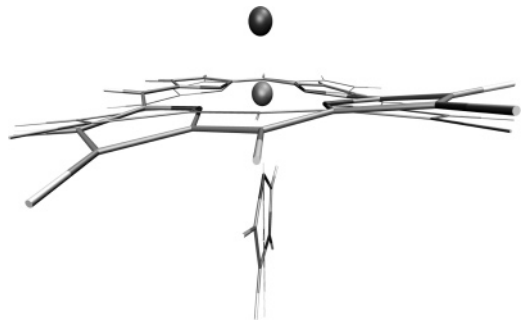

Figure 2. Superimposition of the QM and QM/MM optimized structures for model **1**, in the quartet state. The regular lines correspond to the QM gas-phase geometry and the bold lines to the QM/MM geometry of the QM region. The view in the porphine plane shows the rotation of the proximal ligand and the deformation of the porphine in the QM/MM structure. The RMSD is 0.264 Å; the angle between the imidazoles is 11.8°.

Table 2. Key Distances *R* (in Å) for Cpd I of HRP in Models **1**−**10**

	$R(Fe–N_{ImH})$		R(Fe–O)		$R_{av}(Fe–N_{por})$		Δ	
model	^4A	^2A	^4A	^2A	^4A	^2A	^4A	^2A
1	2.087	2.089	1.669	1.669	2.028	2.027	0.059	0.061
2	2.097	2.099	1.667	1.667	2.028	2.028	0.066	0.067
3	2.094	2.093	1.668	1.668	2.029	2.029	0.063	0.063
4	2.083	2.087	1.668	1.668	2.028	2.028	0.066	0.066
5	2.085	2.085	1.670	1.669	2.028	2.028	0.058	0.059
6	2.072	2.082	1.686	1.686	2.026	2.026	0.065	0.065
7	2.071	2.071	1.683	1.683	2.025	2.025	0.062	0.063
8	2.050	2.050	1.702	1.702	2.024	2.025	0.063	0.063
9	2.060	2.060	1.700	1.700	2.025	2.025	0.069	0.069
10	2.055	2.056	1.700	1.700	2.025	2.025	0.065	0.065

oxo group, the iron and the nitrogen atom of the imidazole ligand (ImH), the average $Fe-N_{Por}$ distance, and the parameter Δ, which measures the deviation of the iron from the average porphyrin plane.

The parameters for the two spin states are virtually identical, which is not surprising in view of the identical energies. The parameters seem to converge for the three largest models **8**−**10**. The Fe−O distance in protein is shorter than that in the gas phase,[17c] and its value of 1.70 Å is identical to the recent X-ray value[8] and somewhat larger than the EXAFS values of 1.62−1.67 Å.[5a,7] Similarly, the $Fe-N_{ImH}$ distance, around 2.06 Å, is close to the X-ray datum of 2.1 Å[8] but larger than the EXAFS values, 1.91−2.00 Å.[5a,7] As we move from **1** to **8**−**10**, one can see a trans effect; the Fe−O bond gets longer while the $Fe-N_{ImH}$ bond gets shorter. Apparently, the hydrogen bonding to the oxo-iron group in the larger models causes elongation of the Fe−O distance with concomitant shrinkage of the $Fe-N_{ImH}$ distance.

C. Spin Densities. Table 3 lists the spin densities for selected atoms and groups in models **1**−**10** obtained from QM/MM calculations with the B2 basis set (B2//B1 data, see Supporting Information for B1 data). The influence of the trans effect is seen in the results for the oxo-iron moiety. The spin densities on iron lie between 1.31*e* and 1.40*e* for models **1**−**5** but increase to 1.44*e*−1.57*e* for models **6**−**10**. At the same time the spin densities on oxygen decrease. Hence, the distal residues (Arg_{38} and His_{42}) affect not only the Fe−O and Fe−N bond lengths (see above) but also the electronic structure of the Fe−O moiety. They make the Fe═O bond more ionic and thereby shift spin density from oxygen to iron. However, the total spin densities on the FeO moiety vary only between 2.03*e* and 2.12*e* and are thus always close to 2.

The imidazole ligand carries little spin density, of the order of 0.01*e*−0.03*e*. The spin density of the third electron is distributed over the porphyrin and other residues, depending on the QM model. For the smallest QM region (**1**), the porphyrin spin density is near unity. When formate is added to the QM subsystem (model **2**), the porphyrin spin density decreases and a small part of the density moves to formate. However, as soon as the latter is screened at the QM level in **4** and **9**, the spin density on formate virtually vanishes again, indicating that the screening residues need to be treated at the QM rather than the MM level in this case. By contrast, the screening effect of the environment on the propionate side chains is already captured by an MM description. Thus, gas-phase QM calculations on the isolated QM region **5** yield significant spin density (−0.63*e* for the doublet state and 0.63*e* for the quartet) on the propionates, while the QM/MM data (B2//B1) for **5** show no spin density on the propionates. Likewise, when the propionate side chains are explicitly screened in QM subsystems **5** and **10**, the propionate spin density is zero. Inspection of the B1 data (see Supporting Information) reveals that the spin density drift from the porphyrin to the side chains and other residues is generally larger for basis set B1: for example, even in **9** there is significant spin density (0.1*e*) on the formate model of Asp_{247}, which however vanishes with the larger basis set, B2. One can thus conclude that *the spin density drift from the porphyrin to the propionate substituents or to side chain residues reflects basis set deficiency and/or improper screening of the negatively charged groups*. Once these two features are treated properly, the spin density drift virtually disappears. This conclusion is consistent with similar findings in the case of Cpd I of cytochrome P450,[20b] where proper screening of the propionates eliminates the spin density, which appears on these groups without such screening. In sum: according to the above results, the electronic structure of HRP Cpd I is in accord with the classical picture shown in Scheme 2, with three unpaired electrons; two on the FeO moiety and the third one on the porphyrin ring.

D. Imidazole−Imidazolate Character of the Proximal Ligand. Since the imidazolate character of the proximal ligand was postulated based on NMR data[12] and suggested as a possible explanation for the small energy splitting between the quartet and doublet states,[17b] we decided to investigate these two tautomers using QM/MM. Figure 3 shows the relaxed scan along the proton-transfer coordinate from the imidazole ligand to the Asp_{247} residue, using model **4**. It is seen that the imidazole tautomer is 14 kcal/mol more stable than the imidazolate species. Furthermore, the imidazolate complex is not a minimum at the QM/MM level. Single-point calculations (B2//B1) yield 11.4 kcal/mol in the quartet state and 11.7 kcal/mol in the doublet state, still a large enough difference to rule out the possibility that the proximal ligand HRP Cpd I is imidazolate.

One may still wonder if the presence of Asp_{247} induces any imidazolate character. To this end, Figure 4 compares the simplest model, **1**, with **4** (minimum in Figure 3) and with the actual imidazolate complex (leftmost point in Figure 3). The inclusion of Asp_{247} in the QM region lengthens the N−H bond of imidazole by 0.02−0.03 Å (**1** vs **4**), but the effect is small in accord with previous gas-phase studies.[17c,18] In both cases the imidazole carries a very small residual spin density of less than 0.03*e*. What is more interesting is the fact that the actual

Table 3. Spin Densities for the Fe and O (oxo) Atoms and for the FeO, Imidazole (ImH), Porphine (Por), and the Other Groups in Models **1**−**10** at QM(UB3LYP/B2//UB3LYP/B1)/MM(CHARMM22) Level

	Fe		O		FeO		ImH		Por		other groups	
model	^{4}A	^{2}A	^{4}A	^{2}A	^{4}A	^{2}A	^{4}A	^{2}A	^{4}A	^{2}A	^{4}A	^{2}A
1	1.317	1.364	0.733	0.734	2.050	2.099	0.019	−0.010	0.931	−1.089	0.019	−0.010
2	1.321	1.403	0.714	0.711	2.035	2.114	0.032	−0.020	0.857	−1.004	0.109	−0.110
3	1.322	1.367	0.714	0.720	2.036	2.087	0.028	−0.004	0.922	−1.056	0.043	−0.031
4	1.316	1.366	0.726	0.726	2.042	2.092	0.025	−0.004	0.933	−1.087	0.025	−0.005
5	1.325	1.377	0.721	0.727	2.046	2.104	0.022	−0.012	0.930	−1.090	0.024	−0.015
6	1.4397	1.4869	0.6345	0.6321	2.074	2.119	0.010	−0.020	0.905	−1.108	0.010	−0.011
7	1.469	1.516	0.575	0.577	2.044	2.094	0.021	−0.009	0.924	−1.098	0.032	0.004
8	1.523	1.576	0.515	0.518	2.037	2.093	0.025	−0.008	0.924	−1.097	0.038	0.004
9	1.526	1.579	0.506	0.510	2.032	2.089	0.032	−0.010	0.921	−1.087	0.047	−0.002
10	1.494	1.550	0.548	0.548	2.042	2.098	0.024	−0.013	0.931	−1.091	0.039	−0.007

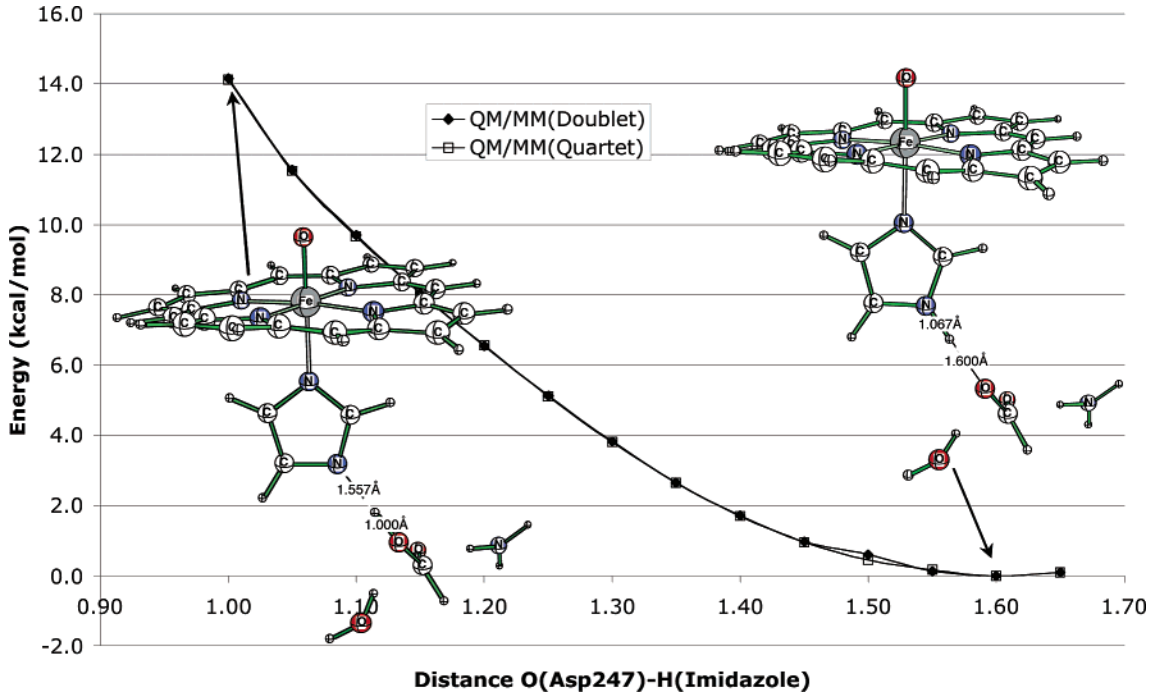

Figure 3. Relaxed scan (QM/MM(UB3LYP)/B1) along the O−H coordinate for the proton transfer from the proximal ligand to Asp_{247}, for the doublet and quartet state. The zero on the energy scale corresponds to the minimum of the imidazole/Asp^- tautomer. Except for the point at a distance of 1.50 Å, the curves for the doublet and quartet are superimposed and thus indistinguishable.

imidazolate complex, on the right-hand side of Figure 4, has only a spin density of 0.06*e*−0.11*e* on the imidazolate ligand, the rest being on the porphyrin. This is no doubt due to the effect of the strong screening by the formic acid model of Asp_{247}. The QM/MM results thus indicate that a putative imidazolate ligand would not carry much radical character in HRP Cpd I, in contrast to the DFT results for a protein-free model.[17b] In an additional test, we added to the QM system in **2** the water molecule (W_{355}) that is hydrogen bonded to Asp_{247} and reoptimized the geometry. The results showed virtually no change in the distances or in the spin density on the His proximal ligand (see the Supporting Information).

E. Assignment of the Electronic Structure of HRP Cpd I. A precise assignment of the ground state of Cpd I, depends on the identity of the third singly occupied orbital in Scheme 2 and on the spin density distribution on the porphine. Figure 5 shows the spin density on the porphine for models **8** and **10**. It is seen that the spin density is largest on the nitrogen atoms and on the *meso* carbon positions, as would be expected for an A_{2u} radical cationic state. However, one finds density also on the various pyrrole carbon positions. This last feature is indicative of some A_{1u} character. Indeed in our previous model calculations,[17c] the A_{1u} states were found to be only 5 kcal/mol higher than the A_{2u} states, such that $A_{2u}-A_{1u}$ mixing can be expected in the absence of symmetry (as in the enzyme).

A closer inspection of the "a_{2u}" natural orbital of model **8** in Figure 6 shows that it has indeed predominantly large contributions on the nitrogen and *meso* positions. But there are also significant contributions on the pyrrole carbon atoms next to the nitrogens, and these contributions are out-of-phase exactly as in the a_{1u} orbital; the β positions of the pyrroles have very small coefficients which are invisible in the figure and correspond to the out-of-phase combination as in the a_{1u} orbital. This finding is perhaps not entirely surprising since Rovira and Fita[38] already reported such behavior and linked it to the Fe−N(ImH) distance; when this distance increased, the a_{1u} character increased and vice versa.

F. Mössbauer Parameters: The isomer shifts, quadrupole splittings, and asymmetry parameters for models **1** and **8** are given in Table 4, alongside the corresponding experimental data.

(38) Rovira, C.; Fita, I. *J. Phys. Chem. B* **2003**, *107*, 5300−5305.

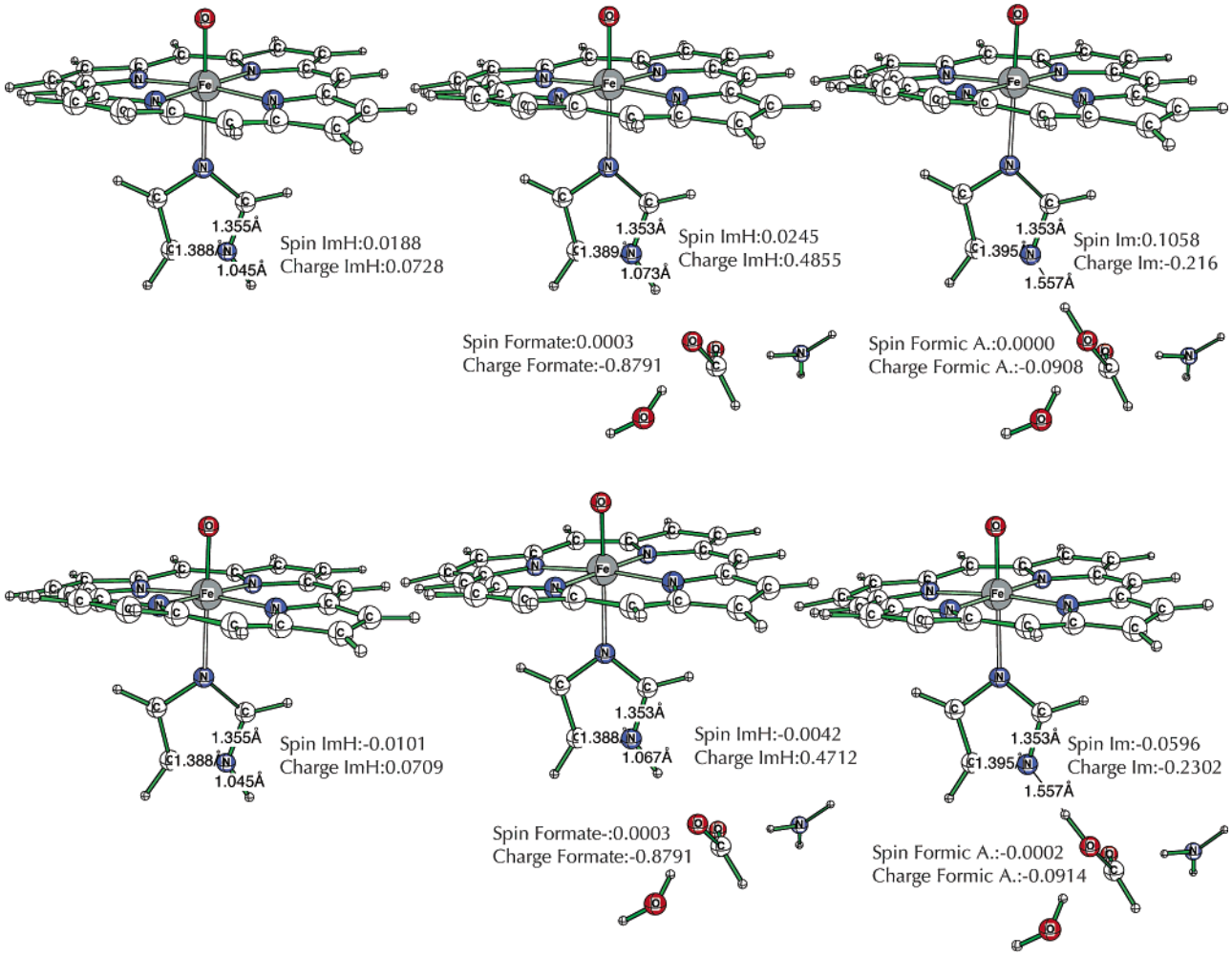

Figure 4. Comparison of the imidazole proximal ligand in the quartet (top) and doublet (bottom) states of **1** (left), **4** (middle), and the imidazolate complex Im^-/AspH (right).

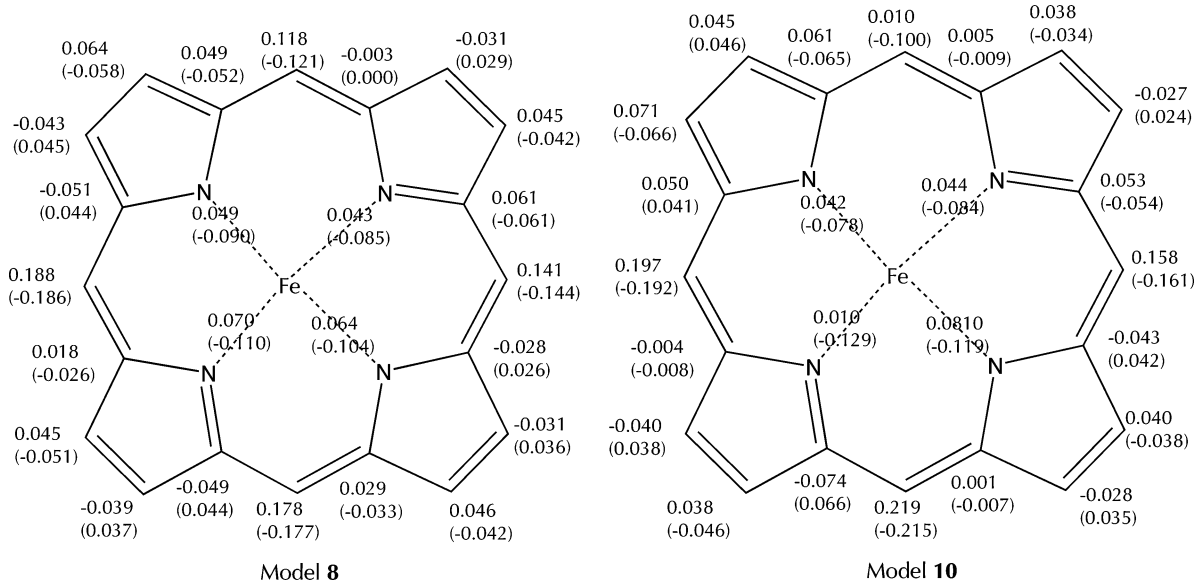

Figure 5. ^4A (^2A) spin density distribution (B2//B1 data) on the porphyrin, in models **8** and **10**.

The calculated quadrupole splittings and asymmetry parameters for **1** differ considerably from the experimental values. They agree much better with experiment when Arg_{38} and His_{42} are included in the QM region (**8**). In view of the expected uncertainties of the computed Mössbauer parameters (±0.1 mm/s for δ, ±0.3 mm/s for ΔE_Q, and ±0.2 for η),[36,39] we

(39) Zhang, Y.; Oldfield, E. *J. Am. Chem. Soc.* **2004**, *126*, 4470−4471.

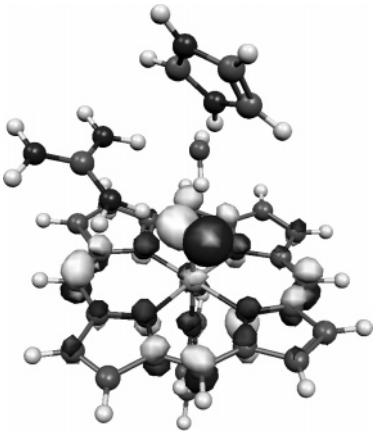

Figure 6. Singly occupied natural orbital of the doub1et state for model **8**, which demonstrates a_{1u} (unpaired spin density only on α and β carbons of pyrroles) and a_{2u} (unpaired spin density only on pyrrolic nitrogens and meso carbons) orbital mixing.

Table 4. Experimental and Calculated Mössbauer Isomer Shift δ (^{57}Fe), Quadrupole Splitting ΔE_Q, and Asymmetry Parameter η for Cpd I of HRP

	experiment	model **1** (^{4}A/^{2}A)	model **8** (^{4}A/^{2}A)
δ (mm/s)	0.08	0.07/0.07	0.03/0.03
ΔE_Q (mm/s)	1.25	0.647/0.666	1.099/1.109
η	0	0.510/0.464	0.106/0.114

conclude that only model **8** is consistent with experiment. The hydrogen-bonding network on the distal side and its interaction with the FeO moiety thus need to be taken into account explicitly in order to reproduce the Mössbauer parameters.

IV. Discussion

The QM/MM calculations of Cpd I of HRP reveal the subtle effects that the protein exerts on the active species. The following discussion will attempt to elucidate these effects one by one.

Most pronounced is the trans effect that elongates the Fe−O bond and shortens the Fe−N_{ImH} bond (Table 2). These changes are attended by a concomitant spin density decrease on oxygen and an increase on iron (Table 3). The factor behind these changes is the hydrogen bond network on the distal side. Compared to **1**−**5**, the Fe−N_{ImH} (Fe−O) bond is shorter (longer) by ca. 0.03 Å in model **8**, which incorporates the essential parts of the hydrogen bonding machinery (His_{42} and Arg_{38}, as well as W_{427} which bridges the two residues to the oxo-ferryl) in the QM subsystem. The additional inclusion of heme side chains and their neighboring residues as well as the environment of proximal histidine has minor geometrical effects (less than 0.01 Å, see **8** vs **9** and **10**). The spin density changes within the Fe−O moiety set in even earlier, and already in model **6** that involves Arg_{38} there is a spin density transfer of $>0.1e$ from oxygen to iron. These changes can be understood using a valence bond (VB) description of the bonding[40] in the oxo-iron moiety, as shown in Figure 7. The Fe═O unit has an electronic structure analogous to $^3O_2$; namely two electrons in the π system have the same spin. In a purely covalent bond as shown in Figure 7a, the bond is described by a mixture of two identical structures, each having a single electron on both iron and oxygen, in both the *xz* and *yz* planes. If the wave function were

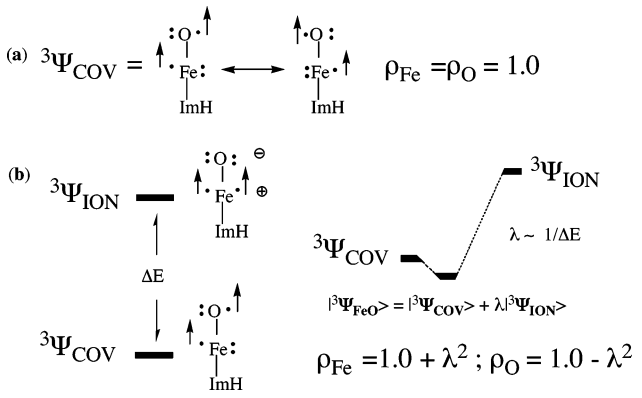

Figure 7. A valence bond diagram for rationalizing spin density (ρ) distribution in the FeO moiety of HRP Cpd I. The *z*-axis is the Fe−O axis. The *xz* and *yz* planes each involve three-electron bonds, responsible for the π-bonding in the FeO moiety: (a) A hypothetical situation of a purely covalent structure; the spin densities on Fe and oxygen are 1.0. (b) A situation that involves mixing of covalent and ionic structures (a single structure of the covalent variety is shown). Here the spin density on Fe exceeds that on oxygen by $2\lambda^2$, where λ is the mixing coefficient of the ionic structure.

indeed purely covalent, the spin density would be one on each of the two atoms. Inspection of Table 2 shows that this is never the case; iron has always a spin of more than one, while oxygen has less than one. This deviation from the covalent picture is due to the admixture of a ionic form, Fe^+—O^-, as shown in Figure 7b. Since the ionic form has two net spins on Fe and none on oxygen, its mixing into the covalent form will increase the spin density on iron at the expense of oxygen, and the spin density shift will depend on the mixing parameter λ (in Figure 7b). In turn λ is inversely proportional to the energy gap, ΔE, between the two VB structures. The presence of the hydrogen-bonding machinery, and especially the positively charged Arg_{38} residue, near the oxygen atom of the FeO moiety, will stabilize the ionic structure preferentially[40,41] and will therefore increase the mixing coefficient, λ, causing thereby an increased spin density shift from oxygen to iron. At the same time, the increased bond ionicity will eventually cause elongation of the Fe═O bond at some critical value of the mixing parameter λ. Since σ-bonding is delocalized over the entire N_{ImH}—Fe—O moiety, the elongation of the Fe—O linkage will be attended by an N_{ImH}—Fe shortening, i.e., a trans effect. Thus, the protein and its interaction with the FeO moiety of the active species cause both the shift in spin density and the trans effect of HRP Cpd I. The effect of the distal hydrogen bonding to the FeO moiety changes the valence state of the iron atom considerably, and may well be responsible for the observation that the reproduction of the experimental Mössbauer parameters requires model **8** but fails with model **1**.

Another interesting effect caused by the protein is the mixed A_{2u}−A_{1u} character of the ground state. Two states can mix if their energy gap is small enough and if the mixing is not prohibited by symmetry. To begin with, due to the small mixing of the imidazole orbitals with a_{2u},[17c] the a_{2u} and a_{1u} orbitals remain almost degenerate, as in the free porphyrin. As such, the gap between the pure A_{2u} and A_{1u} states is very small; it is of the order of 1 kcal/mol in the gas-phase model **1**.[17c] What

(40) Shaik, S.; Hiberty, P. C. *Rev. Comput. Chem.* **2004**, *20*, 1−100.

(41) Note that the effect on charge density will be mitigated by an inverse polarization of the σ(FeO) bond. As such, the spin density is a more sensitive probe of this effect, since it gauges only the π-effects.

the protein does is to distort the structure (see Figure 2) and reduce the symmetry of the porphyrin sufficiently, so that the two states, which are very close in energy, can mix their a_{1u} and a_{2u} orbitals and hence also their characters. This can be contrasted with the situation in Cpd I P450, where the energy gap between A_{2u} and A_{1u} states is large, ca. 20 kcal/mol,[42] due to the strong mixing of the sulfur orbital with the a_{2u} orbital (but not with a_{1u}). Having rationalized the mixed A_{2u}/A_{1u} nature of the ground state of HRP Cpd I, it is important to emphasize that the A_{2u} character is still dominant.

An additional effect exerted by the protein can be appreciated from the electronic structure of model **5**, where the QM region includes the propionate side chain substituents, but not the screening residues. Gas-phase QM calculations on QM region **5** give rise to significant spin density delocalization into the propionate side chains. However, as soon as the screening of the protein residues is included (i.e., in the QM/MM model **5**), the spin density delocalization onto the propionates vanishes. A similar observation was made for P450 Cpd I, in which the screening effect by the protein residues prevents delocalization into the porphyrin substituents.[20b] Other calculations of P450 Cpd I show that, in certain conformations of the screening residues, spin density can drift to the propionates[23,43] or to other residues in the distal and/or proximal sides.[17c] The protein can thus play a role by opening this channel of delocalization by a conformational change that diminishes the screening effect. Our calculations show however that such electron density drift is not a property of stable (screened) structures, but might occur as a transient feature, e.g., in a transition state for electron transfer from a substrate to the porphyrin radical cation. In such a manner[17c] *the propionate side chain may serve as a conduit for electron transfer in substrate oxidation by the peroxidase*.[22]

Another effect of the protein environment concerns the imidazolate character of the proximal ligand. Thus, in the gas phase, the proton-transfer energy from imidazole to aspartate is calculated with the BPW91 functional to be about 1 kcal/mol.[15b] However, in the protein environment, the proton-transfer energy is much larger, 11.4 (^{4}A)/11.7 (^{2}A) kcal/mol at the QM(B2//B1)/MM level. This is clearly an effect of the protein. Looking separately at the QM and QM/MM energies of the proton-transfer process indicates that most of the effect is in the QM part of the QM/MM energy: QM single points on the geometries obtained by QM/MM calculations indicate that the imidazole form is favored by 8.9 (^{4}A)/9.0 (^{2}A) kcal/mol. Relaxing these geometries in the gas phase decreases the gap between the tautomeric forms to 3.7 (^{4}A)/2.9 (^{2}A) kcal/mol, confirming the result previously obtained by Harris and Loew.[15b] It appears therefore that the residues Tyr_{233} and Ile_{244} stabilize Asp_{247} in its anionic form and disfavor the proton uptake; this protein effect constitutes a significant pK_a shift of Asp_{247}.

The impact of the protein environment is made evident also by the fact that even in the actual imidazolate complex in Figure 4, the spin density on the proximal ligand is quite small (0.1*e*), compared with gas-phase models[17a,b] which predict much larger values, up to 0.8*e*. The diminished spin density of the imidazolate in the QM/MM calculations reflects the polarity of the pocket, which stabilizes the anionic form, Im^-, over the radical form, $Im^\bullet$, of the ligand. This behavior is similar to the one discussed for the $S^-/S^\bullet$ character of the thiolate ligand in P450.[20a] However, in the HRP case, the effect is much more pronounced indicating a more polar environment in HRP compared with P450.

Finally, the near-degeneracy of the antiferromagnetic ($^2A_{2u}$) and ferromagnetic states ($^4A_{2u}$) of HRP Cpd I can be contrasted with the somewhat larger energy difference in P450 Cpd I or CPO Cpd I.[11h,15,17b,20a] The nature of the proximal ligand and the interactions with the protein environment combine to produce a localized triradical Cpd I species in HRP, with two electrons in the FeO moiety and the third in the porphyrin, whereas there is some delocalization in P450 Cpd I due to mixing between the thiolate orbital and the porphyrin a_{2u} orbital. This delocalization in P450 decreases the intrinsically small exchange coupling (by further distancing the unpaired electrons) that normally favors high-spin states and increases electron correlation that benefits more the antiferromagnetic low-spin state, as is the case in organic diradicals.[44]

V. Conclusions

The QM/MM calculations on Compound I of HRP reveal the following results: (a) The lowest doublet and quartet states are virtually degenerate, with two unpaired electrons on the FeO moiety and one localized on the porphyrin, which appears in a radical cationic state. (b) The radical cationic state on the porhyrin has a dominant A_{2u} character with a minor A_{1u} component. (c) The key geometric parameters are R(Fe−O) = 1.70 Å and R(Fe−N_{ImH}) = 2.06 Å. (d) The proximal ligand is imidazole and not imidazolate. The spin density on the imidazole ligand is not very different whether the ligand is imidazole or imidazolate. (e) The calculated Mössbauer parameters fit the experimental data if models of the distal residues (i.e., Arg_{38} and His_{42}), which form a hydrogen bonding network to the FeO moiety, are included in the QM region. Most of these features are in accord with experiment, except for the imidazolate character of the proximal ligand deduced from NMR studies.[12] The protein shapes most of these subtle features of HRP Cpd I.

Acknowledgment. The research at HU was supported by the German Federal Ministry of Education and Research (BMBF) within the framework of the German-Israeli Project Cooperation (DIP). The authors thank F. Neese for making his program ORCA available.

Supporting Information Available: Energies and coordinates for all models, as well as spin densities and charges. This material is available free of charge via the Internet at http://pubs.acs.org.

JA0534046

(42) Ogliaro, F.; de Visser, S. P.; Groves, J. T.; Shaik, S. *Angew. Chem., Int. Ed.* **2001**, *40*, 2874−2878; erratum *ibid* 3503.
(43) Altun, A.; Thiel, W.; Cohen, S.; Shaik, S., unpublished data.
(44) Borden, W. T. In *Encyclopedia of Computational Chemistry*; Schleyer, P. v. R.; Allinger, N. L.; Clark, T.; Gasteiger, J.; Kollman, P. A.; Schaefer H. F.; Schreiner, P. R., Eds.; Wiley-Interscience: New York, 1998; Vol. 1, pp 708−722.